Superconductivity between standard types: Multiband versus single-band materials

A. Vagov, A. A. Shanenko, M. V. Milošević, V. M. Axt, V. M. Vinokur, J. Albino Aguiar, and F. M. Peeters

Phys. Rev. B **93**, 174503 — Published 6 May 2016

DOI: 10.1103/PhysRevB.93.174503

Superconductivity between standard types: multi-band versus single-band materials

A. Vagov,[1] A. A. Shanenko,[2] M. V. Milošević,[3] V. M. Axt,[1] V. M. Vinokur,[4] J. Albino Aguiar,[2] and F. M. Peeters[3]

[1]*Institut für Theoretische Physik III, Bayreuth Universität, Bayreuth 95440, Germany*
[2]*Departamento de Física, Universidade Federal de Pernambuco, Av. Jorn. Aníbal Fernandes, s/n, 50740-901, Recife-PE, Brazil*
[3]*Departement Fysica, Universiteit Antwerpen, Groenenborgerlaan 171, B-2020 Antwerpen, Belgium*
[4]*Materials Science Division, Argonne National Laboratory, USA*

In the nearest vicinity of the critical temperature, types I and II of conventional single-band superconductors interchange at the Ginzburg-Landau parameter $\kappa = 1/\sqrt{2}$. At lower temperatures this point unfolds into a narrow but finite interval of κ's, shaping an inter-type (transitional) domain in the (κ, T)-plane. In the present work, based on the extended Ginzburg-Landau formalism, we show that the same picture of the two standard types with the transitional domain in between applies also to multi-band superconductors. However, the inter-type domain notably widens in the presence of multiple bands and can become extremely large when the system has a significant disparity between the band parameters. It is concluded that many multi-band superconductors, such as recently discovered borides and iron-based materials, can belong to the inter-type regime.

PACS numbers: 74.25.-q,74.25.Dw,74.25.Ha,74.70.Ad,74.70.Xa

I. INTRODUCTION

Observation of non-conventional vortex configurations in MgB_2[1] has ignited the interest to possible superconductivity types in multi-band superconductors, where many carrier bands contribute to the condensate state. In single-band materials the distinction between the types is routinely explained by employing the Ginzburg-Landau (GL) theory[2–4] which distinguishes ideally diamagnetic type-I materials and type-II superconductors that allow for the mixed state. Following this theory the interchange between the types occurs when the GL parameter $\kappa = \lambda_L/\xi$ crosses its critical value $\kappa_0 = 1/\sqrt{2}$ (λ_L is the London magnetic penetration depth, ξ is the GL coherence length).[3] A key difference that distinguishes those types is the vortex-vortex interaction: it is repulsive in type II and attractive in type I superconductors. At $\kappa = \kappa_0$, referred to as the Bogomolnyi point, vortices do not interact. This is a consequence of the fact that the GL theory at this point reduces to a pair of the first order self-dual Bogomolnyi equations.[5,6] The self-duality, first discussed in the context of cosmological strings,[5,7] leads to an infinite degeneracy of different flux configurations,[6,8,9] from which the absence of the vortex-vortex interactions follows.

However, detailed experimental investigations[10] as well as theoretical calculations beyond the GL theory[11–15] show that the GL dichotomy of the superconductivity types is achieved only in the limit $T \to T_c$ (T_c is the critical temperature). At $T < T_c$ the Bogomolnyi point unfolds into a finite temperature-dependent interval of κ's (in this paper referred to as the inter-type/transitional interval or domain), where superconductivity cannot be attributed to one of the standard types. For example, superconductors in this interval reveal the first order phase transition between the Meissner and mixed states at H_{c1} and, plausibly, between the mixed and normal states at H_{c2}.[11,15] Theoretical modeling, based on microscopic BCS as well as on the Neumann-Tewordt (NT)[16] theories, has led to a general perception that the key characteristic of the transitional domain, that is responsible for its non-standard properties, is the non-monotonic vortex-vortex interaction: the long-range attraction combined with the short-range repulsion.[11,12,15] It was argued that such attraction is a manifestation of non-local effects that are not inherent to the GL theory.[17] Being a few, and outside the GL description, single-band materials in the narrow inter-type domain are, as a rule, ignored in textbooks and the corresponding magnetic response remains scarcely investigated to date.

Although the unconventional vortex patterns in MgB_2[1] were also attributed to a long-range vortex attraction, the proposed explanation was totally different. It was conjectured in this case that it appears due to the interplay between different carrier bands or, more precisely, due to a competition between different length-scales of π- and σ-bands in MgB_2.[18] This explanation has led to a controversial idea of a new superconductivity type found only in multi-band systems.[1,18]

Critics of this concept pointed to similarities between the flux configurations observed in MgB_2 and in the inter-type regime of single-band superconductors.[17] They also noted inconsistencies of the multi-component GL equations[19,20] employed for analysis of vortex matter in MgB_2, where the different band gaps were treated as components of the Landau order parameter.[18,21] In particular, it is well known that the Landau theory for phase transitions relates the number of the order-parameter components not to the number of bands but to the dimension of the corresponding irreducible representation of the symmetry group.[22,23]

To this date it remains unclear if explanation of the nonstandard vortex distributions in MgB_2 requires a specific multi-band mechanism or the underlying physics is similar to that of single-band superconductors in the transitional interval.[17] More generally, classifying super-

conductivity types and their interchange in multi-band systems remains an unresolved issue. In the present work we address this problem with the extended GL (EGL) formalism[20,24] derived as the exact perturbation expansion of the BCS theory over the small proximity to the critical temperature $\tau = 1 - T/T_c$ to one order beyond the standard GL approach. It is important that this correction not only improves the accuracy of the calculations but also captures phenomena that cannot be described within the standard GL theory. In particular, this concerns the inter-type domain absent in the GL picture.

We demonstrate that unless the system has some additional band symmetry,[25] multi-band superconductors obey the standard classification with the two superconductivity types and the transitional domain in between. The inter-type behavior has the same origin for both multi- and single-band superconductors, namely, it appears as a result of lifting the Bogomolnyi point degeneracy. However, the crucial difference of systems with multiple bands is that the transitional domain notably widens and can become extremely large when disparity between microscopic characteristics of contributing bands is significant. Thus, many of multi-band superconductors can belong to the inter-type regime.

Presentation of our results is separated into two main parts. In the first part (Sec. II) we discuss the transitional domain in single-band superconductors. The EGL formalism is formulated in the universal form independent of the number of bands and thus analysis of the single- and multi-band cases are qualitatively similar. Presenting first a simpler single-band case helps to better understand the phenomenon of the inter-type superconductivity and is also needed for highlighting similarities and differences between the single- and multi-band superconductors. The current understanding of the inter-type regime even in the single-band case remains sketchy and contradictory and calls for revisiting the problem.

The second part of the paper (Sec. III) extends our consideration to the multi-band case. Here explicit calculations are done for a two-band superconductor, where most of results can be obtained analytically. We argue that qualitatively similar conclusions hold also for any number of carrier bands.

For the convenience of the reader technical details of our calculations are given in Appendices.

II. SINGLE-BAND SYSTEMS

Let us briefly summarize the past achievements and related problems in description of the inter-type regime in single-band superconductors. Studying the transitional domain between types I and II requires an approach going beyond the GL theory. Solving equations of the fully microscopic formalism is very demanding numerically due to inhomogeneity of the mixed state. This is the reason why microscopic analysis has been performed only for few selected problems, in particular, to calculate outer boundaries of the transitional domain:[13,14] the upper boundary is determined by the onset of the long-range vortex-vortex attraction and the lower one is set by appearance/disappearance of the mixed state.

A compromise between the microscopic theory and the GL approach is the Neumann-Tewordt (NT) theory,[16] which has been used to obtain most of currently known results on the inter-type superconducting behavior. This formalism was originally derived from the so-called local approximation for the BCS theory and yields the free energy functional, where the GL contribution is augmented by the terms with higher order derivatives and higher non-linearity. The NT approach was used to calculate outer boundaries of the transitional domain[11,12,15] but also demonstrated the presence of other boundaries introducing subdivisions in the transitional domain and inter-type superconducting behavior. Unfortunately, consequences of such subdivisions did not receive much attention in the literature.

However, the NT theory has several fundamental difficulties. First, highly non-linear equations of this formalism are in fact not much simpler than the original microscopic theory.[16,26–28] Second, it may lead to nonphysical results such as a rapidly oscillating order parameter in the single-vortex solution.[27,28] In order to simplify the analysis, the NT equations were linearized by seeking its solution in the form of a small correction to the solution of the GL equations.[11,12] Corrections to the GL free energy were also obtained by substituting the GL solution directly into the NT functional.[15] However, results of both approaches for the boundaries of the inter-type domain were considerably different (see Tab. I). This must be taken into consideration together with the fact that the nonphysical results of the full NT equations can also cast doubts on their linearized version.

Here we revisit the problem of the inter-type superconductivity in single-band materials using the EGL formalism[20,24] derived perturbatively (in $\tau = 1 - T/T_c$). An essential advantage of our approach is the possibility to obtain universal analytical expressions for the characteristics of the transitional domain in both single- and multi-band systems. As mentioned above, accounting for the terms beyond the standard GL approach in the τ-expansion allows one to access novel physics not captured in the GL picture. The accuracy of the EGL formalism is established by comparing with the results of the full microscopic theory, which was done in Refs. 20 and 24 for some pertinent quantities, as well as with the available experimental data, see Fig. 2 below.

A. Criteria for interchange of types I and II

We start the analysis of the transitional domain with the general remark that the superconductivity types are related to the way how the magnetic field penetrates the bulk superconductor and produces a non-uniform configuration of the flux/condensate. Specifying such a con-

figuration is not important in the extreme cases where $\kappa \gg 1$ or $\kappa \ll 1$, neither in the limit $T \to T_c$. However, the situation changes for $\kappa \sim 1$ and $T < T_c$, where choosing different variants of a non-uniform magnetic flux distribution gives rise to different scenarios of the interchange between types I and II.

A criterion for such interchange utilizes the corresponding Gibbs free energy: when it becomes smaller than that of the Meissner state at the thermodynamic critical field H_c, the flux/condensate configuration in question can appear.[4] The respective difference between the Gibbs free energies is written as

$$\mathfrak{G} = \int \mathfrak{g}\, d\mathbf{r}, \quad \mathfrak{g} = \mathfrak{f} + \frac{H_c^2}{8\pi} - \frac{H_c B}{4\pi}, \tag{1}$$

where $\mathfrak{f}$ is the free-energy density of the corresponding non-uniform state and the magnetic field $\mathbf{B}$ is parallel to the external magnetic field of value H_c. The onset of this non-uniform state is found from the equation

$$\mathfrak{G}(\kappa, T) = 0 \tag{2}$$

that yields the corresponding GL critical parameter $\kappa^*(T)$, hereafter referred to as a simply critical parameter. On the (κ, T)-plane $\kappa^*(T)$ separates domains with and without the flux/condensate configuration of interest, that are called types II and I.

Several types of such non-uniform flux configurations are traditionally employed in order to construct the criterion of the type interchange. Most common is the domain wall (interface) between superconductive (S) and normal (N) phases.[3,4] The interchange takes place when the surface energy associated with the domain wall becomes zero. Another criterion is obtained by considering the superconductivity nucleation at the upper critical field H_{c2}: here types I and II interchange when $H_{c2} = H_c$.[3,4] The stability of a single Abrikosov vortex is also useful, resulting in the interchange condition $H_{c1} = H_c$.[3,4] In addition, it is also possible to associate the type interchange with a certain property of a chosen flux configuration. For example, in the context of the unconventional vortex states, discussed in Introduction, one can consider interaction of two Abrikosov vortices that is repulsive in type II and attractive in type I.[3,4] The corresponding criterion is a change of the sign of the vortex-vortex interaction or, more precisely, of its long-range asymptote.

Within the standard GL theory the differences between the above criteria are irrelevant: one obtains the same temperature-independent critical parameter $\kappa^* = \kappa_0$. Superconductivity types I and II are found at $\kappa < \kappa_0$ and $\kappa > \kappa_0$, respectively, while switching between types I and II takes place sharply at $\kappa = \kappa_0$. At this point differences between types I and II disappear due to an infinite topological degeneracy of the GL theory. This degeneracy was first noted in the context of the so-called Sarma solution,[3] however, its comprehensive analysis was done only later by Bogomolnyi in relation to the physics of cosmic strings.[5,6]

As already mentioned in the Introduction, the classification based on the GL theory is strictly valid only in the limit $T \to T_c$. At $T < T_c$ corrections to the GL theory remove the degeneracy, leading to that different criteria for the type interchange give different critical parameters.[11,13,15] In particular, conditions $H_c = H_{c2}$ and $H_c = H_{c1}$ correspond to κ_2^* and κ_1^*, respectively. The zero surface energy yields κ_s^* whereas changing the sign of the long-range vortex interaction gives κ_{li}^*. All temperature-dependent critical parameters converge to κ_0 at $T \to T_c$, manifesting the degeneracy of the Bogomolnyi point (κ_0, T_c). At $T < T_c$ there is a finite interval of κ's where the superconducting magnetic response cannot be classified as belonging to one of the standard types. Thus, in the (κ, T)-plane superconductivity types I and II are separated by the transitional (or inter-type) domain.

B. Gibbs free energy difference

We calculate the Gibbs free-energy difference $\mathfrak{G}$ in Eqs. (1) and (2) using the EGL formalism.[24] In this approach the free energy is given by a series in $\tau = 1 - T/T_c$, obtained by expanding all pertinent physical quantities. The spatial coordinates are scaled as $\tau^{1/2}\mathbf{r}$, which introduces the corresponding scaling into the spatial derivatives. The gap function Δ and the magnetic field $\mathbf{B}$ (or the vector potential $\mathbf{A}$) are represented in the form

$$\begin{aligned} \Delta &= \tau^{1/2}\big(\Psi + \tau\psi + \dots\big), \\ \mathbf{B} &= \tau\big(\mathfrak{B} + \tau\mathfrak{b} + \dots\big), \\ \mathbf{A} &= \tau^{1/2}\big(\mathfrak{A} + \tau\mathfrak{a} + \dots\big). \end{aligned} \tag{3}$$

The free-energy density is found as[24]

$$\mathfrak{f} = \tau^2\big(\mathfrak{f}^{(0)} + \tau\mathfrak{f}^{(1)} + \dots\big), \tag{4}$$

where the lowest-order contribution represents the standard GL free-energy functional

$$\mathfrak{f}^{(0)} = \frac{\mathfrak{B}^2}{8\pi} + a\big|\Psi\big|^2 + \frac{b}{2}\big|\Psi\big|^4 + \mathcal{K}\big|\mathfrak{D}\Psi\big|^2, \tag{5}$$

with $\mathfrak{D} = \boldsymbol{\nabla} - \mathbb{i}2e\mathfrak{A}/(\hbar\,\mathbb{c})$ the gauge-invariant derivative. The leading-order corrections to the GL free energy are split into two parts

$$\mathfrak{f}^{(1)} = \mathfrak{f}_1^{(1)} + \mathfrak{f}_2^{(1)}, \tag{6}$$

where the first part is given by

$$\begin{aligned} \mathfrak{f}_1^{(1)} =& \frac{a}{2}\big|\Psi\big|^2 + 2\mathcal{K}\big|\mathfrak{D}\Psi\big|^2 + b\big|\Psi\big|^4 + \frac{b}{36}\,\frac{e^2\hbar^2}{m^2\mathbb{c}^2}\mathfrak{B}^2\big|\Psi\big|^2 \\ &- \mathcal{Q}\Big\{\big|\mathfrak{D}^2\Psi\big|^2 + \frac{1}{3}(\mathrm{rot}\,\mathfrak{B}\cdot\mathbb{i}) + \frac{4e^2}{\hbar^2\mathbb{c}^2}\mathfrak{B}^2\big|\Psi\big|^2\Big\} \\ &- \frac{\mathcal{L}}{2}\Big\{8\,|\Psi|^2\big|\mathfrak{D}\Psi\big|^2 + \big[\Psi^2(\mathfrak{D}^*\Psi^*)^2 + \mathrm{c.c.}\big]\Big\} \\ &- \frac{c}{3}\big|\Psi\big|^6, \end{aligned} \tag{7}$$

and includes only the lowest-order contributions Ψ and $\mathfrak{B}$ ($\mathfrak{A}$) to the gap and field, respectively, while the second part writes

$$\mathfrak{f}_2^{(1)} = \frac{(\mathfrak{B}\cdot\mathfrak{b})}{4\pi} + \big(a + b|\Psi|^2\big)(\Psi^*\psi + \text{c.c.}) + \mathcal{K}\left\{\big(\mathfrak{D}\,\Psi\cdot\mathfrak{D}^*\psi^* + \text{c.c.}\big) - \big(\mathfrak{a}\cdot\mathfrak{i}\big)\right\}, \quad (8)$$

and contains also the leading corrections to the gap and field, ψ and $\mathfrak{b}$ ($\mathfrak{a}$). In Eqs. (7) and (8)

$$\mathfrak{i} = \mathbb{i}\frac{2e}{\hbar\,\mathbb{c}}\big(\Psi\,\mathfrak{D}^*\,\Psi^* - \Psi^*\,\mathfrak{D}\,\Psi\big), \quad (9)$$

where $\mathcal{K}\mathbb{c}\mathfrak{i}$ is the lowest-order contribution to the supercurrent density.

Coefficients in Eqs. (4) - (8) are obtained using a chosen microscopic model of the charge-carrier states. In particular, for a spherical Fermi surface in the clean limit one gets

$$a = -N(0), \quad b = N(0)\frac{7\zeta(3)}{8\pi^2 T_c^2}, \quad c = N(0)\,\frac{93\zeta(5)}{128\pi^4 T_c^4}, \quad \mathcal{K} = \frac{b}{6}\hbar^2 v_F^2, \quad \mathcal{Q} = \frac{c}{30}\hbar^4 v_F^4, \quad \mathcal{L} = \frac{c}{9}\hbar^2 v_F^2, \quad (10)$$

where $N(0) = mk_F/(2\pi^2\hbar^2)$ is the density of the carrier states (DOS) at the Fermi surface with the Fermi-momentum k_F and Fermi-velocity $v_F = \hbar k_F/m$.

A stationary point of the functional given by Eq. (4) yields the main equations of the formalism. The GL equations are obtained as the stationary condition for the lowest-order contribution to the free energy, i.e.,

$$\frac{\delta\mathfrak{F}^{(0)}}{\delta\Psi} = \frac{\delta\mathfrak{F}^{(0)}}{\delta\mathfrak{A}} = 0, \quad (11)$$

where $\mathfrak{F}^{(n)} = \int \mathfrak{f}^{(n)} d\mathbf{r}$, with $n = 0, 1$. Equations for ψ and $\mathfrak{b}$ ($\mathfrak{a}$) read

$$\frac{\delta\mathfrak{F}^{(1)}}{\delta\Psi} = \frac{\delta\mathfrak{F}^{(1)}}{\delta\mathfrak{A}} = 0. \quad (12)$$

Notice, that $\delta\mathfrak{F}^{(1)}/\delta\psi = 0$ and $\delta\mathfrak{F}^{(1)}/\delta\mathfrak{a} = 0$ also generate the GL equations.

One can see that the leading correction to the free energy (i.e., the term $\sim \tau^3$) can be rearranged at the stationary point so that the terms with ψ and $\mathfrak{b}$ ($\mathfrak{a}$) are excluded. This follows from that $\mathfrak{f}_2^{(1)}$ in Eq. (8) is linearly proportional to the functional derivatives $\delta\mathfrak{F}^{(1)}/\delta\psi$ and $\delta\mathfrak{F}^{(1)}/\delta\mathfrak{a}$ (up to some vanishing surface integrals) that are zero by virtue of Eq. (12). Therefore, at the stationary point the leading correction to free energy is reduced to Eq. (7). Using solutions to the GL equations (11), we find the free energy density from Eqs. (4) - (8) and then calculate the Gibbs free energy difference given by Eq. (1).

Calculating the Gibbs free energy difference up to the leading correction to the GL result requires obtaining the thermodynamic critical field H_c with the same accuracy, which gives[24]

$$H_c = \tau\left(H_c^{(0)} + \tau H_c^{(1)} + \dots\right), \quad (13)$$

where

$$H_c^{(0)} = \sqrt{\frac{4\pi a^2}{b}}, \quad \frac{H_c^{(1)}}{H_c^{(0)}} = -\frac{1}{2} - \frac{ac}{3b^2}. \quad (14)$$

It is convenient to do further calculations using the dimensionless quantities

$$\tilde{\mathbf{r}} = \frac{\mathbf{r}}{\lambda_L\sqrt{2}}, \quad \tilde{\mathfrak{A}} = \kappa\frac{\mathfrak{A}}{H_c^{(0)}\lambda_L}, \quad \tilde{\mathfrak{B}} = \kappa\sqrt{2}\frac{\mathfrak{B}}{H_c^{(0)}}, \quad \tilde{\Psi} = \frac{\Psi}{\Psi_0}, \quad \tilde{\mathfrak{i}} = \frac{4\pi\mathcal{K}\lambda_L}{H_c^{(0)}}\,\mathfrak{i}, \quad \tilde{\mathfrak{f}} = \frac{4\pi\mathfrak{f}}{H_c^{(0)2}}, \quad \tilde{\mathfrak{g}} = \frac{4\pi\mathfrak{g}}{H_c^{(0)2}}, \quad \tilde{\mathfrak{G}} = \frac{4\pi\mathfrak{G}}{H_c^{(0)2}(\lambda_L\sqrt{2})^3}, \quad (15)$$

where

$$\Psi_0 = \sqrt{\frac{|a|}{b}}, \ \lambda_L^2 = \frac{\hbar^2\mathbb{c}^2 b}{32\pi e^2\mathcal{K}|a|}, \ \kappa = \frac{\lambda_L}{\xi} = \frac{\lambda_L|a|}{\mathcal{K}}. \quad (16)$$

Notice that as we use the τ-scaled spatial coordinates, the GL coherence length ξ and the London penetration depth λ_L are scaled accordingly. In the following we write the dimensionless quantities introduced in Eq. (15) without tilde unless it causes any confusion.

The density of the Gibbs free energy difference is given by the expansion

$$\mathfrak{g} = \tau^2\big(\mathfrak{g}^{(0)} + \tau\mathfrak{g}^{(1)} + \dots\big), \quad (17)$$

where in the lowest order we have the GL contribution

$$\mathfrak{g}^{(0)} = \frac{1}{2}\left(\frac{\mathfrak{B}}{\kappa\sqrt{2}} - 1\right)^2 + \frac{1}{2\kappa^2}\,|\mathfrak{D}\Psi|^2 - |\Psi|^2 + \frac{1}{2}\,|\Psi|^4, \quad (18)$$

(now we have $\mathfrak{D} = \boldsymbol{\nabla} + \mathbb{i}\mathfrak{A}$) while the leading correction writes

$$\mathfrak{g}^{(1)} = \left(\frac{\mathfrak{B}}{\kappa\sqrt{2}} - 1\right)\left[\frac{1}{2} + \tilde{c}\right] - \frac{\big|\Psi\big|^2}{2} + \frac{\big|\mathfrak{D}\Psi\big|^2}{\kappa^2} + \big|\Psi\big|^4 + \frac{\tilde{\mathcal{Q}}}{4\kappa^4}\Big\{\big|\mathfrak{D}^2\Psi\big|^2 + \frac{1}{3}(\text{rot}\,\mathfrak{B})^2 + \mathfrak{B}^2\big|\Psi\big|^2\Big\} + \frac{\tilde{\mathcal{L}}}{4\kappa^2}\Big\{8\big|\Psi\big|^2\big|\mathfrak{D}\Psi\big|^2 + \big[\Psi^2(\mathfrak{D}^*\Psi^*)^2 + \text{c.c.}\big]\Big\} + \tilde{c}\,\big|\Psi\big|^6, \quad (19)$$

with the dimensionless coefficients

$$\tilde{c} = \frac{ca}{3b^2}, \quad \tilde{\mathcal{Q}} = \frac{\mathcal{Q}a}{\mathcal{K}^2}, \quad \tilde{\mathcal{L}} = \frac{\mathcal{L}\,a}{b\,\mathcal{K}}. \quad (20)$$

Since we are interested in the near-Bogomolnyi regime, it is also useful to introduce the expansion over $\delta\kappa = \kappa - \kappa_0$, following the suggestion of Ref. 15. Expanding Eq. (2) with respect to $\delta\kappa$ we obtain

$$\mathfrak{G} = \tau^2\Big(\mathfrak{G}^{(0)} + \frac{d\mathfrak{G}^{(0)}}{d\kappa}\,\delta\kappa + \mathfrak{G}^{(1)}\,\tau + \dots\Big), \tag{21}$$

and the coefficients in this expansion are calculated at $\kappa = \kappa_0$, i.e., we incorporate a solution to the GL formalism at κ_0 where it is reduced to the first-order Bogomolnyi equations. The terms $\propto \tau\,\delta\kappa$ are neglected in Eq. (21) because both quantities $\delta\kappa$ and τ are of the same order of magnitude, $\delta\kappa \sim \tau$.

The derivative $d\mathfrak{G}^{(0)}/d\kappa$ contains the direct contribution coming from the explicit appearance of κ in the expression for $\mathfrak{g}^{(0)}$ (the partial derivative below) and the indirect one related to the derivatives $d\Psi/d\kappa$ and $d\mathfrak{A}/d\kappa$. However, one can immediately see that the indirect contribution is equal zero. Namely, the corresponding terms in the integrand are proportional to $\delta\mathfrak{G}^{(0)}/\delta\Psi$ and $\delta\mathfrak{G}^{(0)}/\delta\mathfrak{A}$. These terms disappear because the functional derivatives of $\mathfrak{G}^{(0)}$ are equal to the corresponding functional derivatives of $\mathfrak{F}^{(0)}$ that are zero at the stationary point, see Eq. (11). The final expression for $d\mathfrak{G}^{(0)}/d\kappa$ reads

$$\frac{d\mathfrak{G}^{(0)}}{d\kappa} = \int \frac{\partial\mathfrak{g}^{(0)}}{\partial\kappa}\,d\mathbf{r}, \tag{22}$$

with

$$\frac{\partial\mathfrak{g}^{(0)}}{\partial\kappa} = -\frac{\mathfrak{B}}{\kappa^2\sqrt{2}}\left(\frac{\mathfrak{B}}{\kappa\sqrt{2}} - 1\right) - \frac{1}{\kappa^3}\big|\mathfrak{D}\,\Psi\big|^2. \tag{23}$$

At $\kappa = \kappa_0$ solutions to the GL equations are obtained using the Bogomolnyi self-duality equations (A13) - (A14), that are also used to simplify the integrals in $\mathfrak{G}$. After straightforward but lengthy calculations one obtains for $\mathfrak{G}$ the following general expression:

$$\begin{aligned}\mathfrak{G} =& \tau^2\Big\{ -\sqrt{2}\,\mathcal{I}\,\delta\kappa + \tau\Big[\big(1 - \tilde{c} + 2\tilde{\mathcal{Q}}\big)\,\mathcal{I} \\ &+ \Big(2\,\tilde{\mathcal{L}} - \tilde{c} - \frac{5}{3}\,\tilde{\mathcal{Q}}\Big)\mathcal{J}\Big] + \dots\Big\},\end{aligned} \tag{24}$$

with

$$\mathcal{I} = \int |\Psi|^2\big(1 - |\Psi|^2\big)d\mathbf{r},\ \mathcal{J} = \int |\Psi|^4\big(1 - |\Psi|^2\big)d\mathbf{r}. \tag{25}$$

Details of the solving procedure for the relevant non-uniform flux configurations are discussed in Appendices B and C. It is important that the lowest-order term $\mathfrak{G}^{(0)}$ is zero for any solution of the GL equations at $\kappa = \kappa_0$, manifesting the degeneracy of the Bogomolnyi point. Thus, Eq. (24) comprises only two contributions, $\propto \delta\kappa$ and $\propto \tau$.

C. Critical GL parameters

Substituting Eq. (24) into Eq. (2) one obtains the general expression for critical parameters up to the leading correction in τ, i.e.,

$$\kappa^* = \kappa_0\left\{1 + \tau\,\left[1 - \tilde{c} + 2\tilde{\mathcal{Q}} + \frac{\mathcal{J}}{\mathcal{I}}\left(2\,\tilde{\mathcal{L}} - \tilde{c} - \frac{5}{3}\,\tilde{\mathcal{Q}}\right)\right]\right\}. \tag{26}$$

This expression generalizes our earlier result for the N-S wall solution[24] to an arbitrary flux configuration. The dimensionless constants in Eq. (26) are calculated from Eq. (10), which gives

$$\tilde{c} = -0.227, \quad \tilde{\mathcal{L}} = -0.454, \quad \tilde{\mathcal{Q}} = -0.817. \tag{27}$$

These constants do not depend on the material parameters T_c, $N(0)$ and v_F, which points to the robustness of the approach: one can generally expect that the results are not very sensitive to details of a particular microscopic model, at least for weak disorder.

Using Eq. (26), we calculate the critical parameters for the above criteria of the type interchange. The first criterion is based on the appearance of a flat N-S domain wall. The corresponding solution, outlined in Appendix B, yields $\mathcal{J}/\mathcal{I} = 0.559$. The critical parameter is thus obtained as

$$\kappa_s^* = \kappa_0(1 - 0.027\tau). \tag{28}$$

The condition $H_c = H_{c1}$ is related to the thermodynamic stability of an isolated Abrikosov vortex, the solution to which yields $\mathcal{J}/\mathcal{I} = 0.735$, see Appendix C. The corresponding critical parameter is

$$\kappa_1^* = \kappa_0(1 + 0.093\tau). \tag{29}$$

The condition of changing the sign of the long-range vortex-vortex interaction is calculated using $\mathfrak{G}$ for the state with two single-quantum vortices separated by distance R. Details and the asymptote of $\mathfrak{G}$ at large R are given in Appendix C. Using those results we find $\mathcal{J}/\mathcal{I} \to 2\,(R \to \infty)$ and then the critical parameter reads

$$\kappa_{li}^* = \kappa_0(1 + 0.95\tau). \tag{30}$$

Finally, onset of the superconductivity nucleation is defined by the condition $H_{c2} = H_c$. In order to solve this equation, one can find the upper critical field H_{c2} using the condition of the first appearance of a non-zero gap. Alternatively, one can use Eq. (26) and utilize the fact that in the limit $B \to H_{c2}$ the order parameter Ψ vanishes. Then, as follows from Eq. (25), the integrands for $\mathcal{I}$ and $\mathcal{J}$ are reduced respectively to $|\Psi|^2$ and $|\Psi|^4$. Thus, in this limit one obtains $J/I \to 0$ and the corresponding critical parameter writes

$$\kappa_2^* = \kappa_0(1 - 0.407\tau). \tag{31}$$

	$\frac{d\kappa^*_{li}}{d\tau}$	$\frac{d\kappa^*_1}{d\tau}$	$\frac{d\kappa^*_s}{d\tau}$	$\frac{d\kappa^*_2}{d\tau}$
EGL	0.6726	0.066	-0.019	-0.288
NT-1[11]	0.675	0.065	-0.019	-0.288
NT-2[15]	-0.163	-0.242	-0.254	-0.290

TABLE I. The τ-derivative of the critical parameter κ^* calculated for the different interchange criteria mentioned in the text: comparison between the results of the EGL formalism and NT calculations from Refs. 11 and 15.

One can check that an independent calculation based on a solution to the linearized GL equation for the order parameter yields the same result.

Equations (28) - (31) illustrate that different criteria of the type interchange produce different critical parameters at $T < T_c$. This difference has been noticed earlier in the analysis based on the NT theory.[11,15] However, as mentioned above, there was no agreement on the values of the critical parameters obtained by different versions of the linearization procedure. In Tab. I we provide a summary of the results obtained in the present and earlier works. One can see that our values for the critical parameters coincides with those of Ref. 11, denoted as "NT-1" in Tab. I. However, results of the other approach[15] ("NT-2") are notably different for all critical parameters with the exception of κ_2^*.

The accuracy of our approach is further confirmed by the comparison with the microscopic calculations shown in Fig. 1 which plots results for κ^*_{li} obtained by the EGL and Eilenberger equations.[13] The results of the full non-linear NT theory are also provided.[29] The microscopic data are obtained with numerical uncertainties, illustrated in Fig. 1 by the trust interval between two solid curves. At higher temperatures, $0.7 \lesssim T/T_c \lesssim 1$, all three approaches yield close values, converging to κ_0 in the GL limit $T \to T_c$. However, when the temperature is lowered, $T/T_c \lesssim 0.7$, the NT theory starts to deviate notably from the microscopic solution. On the contrary, the EGL line remains in a good quantitative agreement with the microscopic theory at temperatures down to $T/T_c \sim 0.3$. The EGL approach demonstrates a wider validity domain than the non-linear NT theory. This is because the accuracy of the solution to the non-linear NT theory exceeds the accuracy of its derivation procedure, as was mentioned already in Ref. 28.

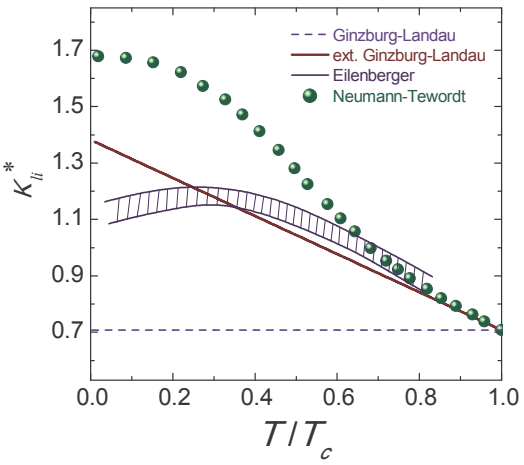

FIG. 1. (Color online) The critical parameter κ^*_{li} (controlling the long-range vortex-vortex attraction) as calculated from Eq. (30), from the Eilenberger equations[13], and from the NT approach.[29] Numerical uncertainties in microscopic calculations are given by the trust interval (shaded area between the upper and lower curves). The standard GL result $\kappa = \kappa_0$ is represented by the dashed line for reference.

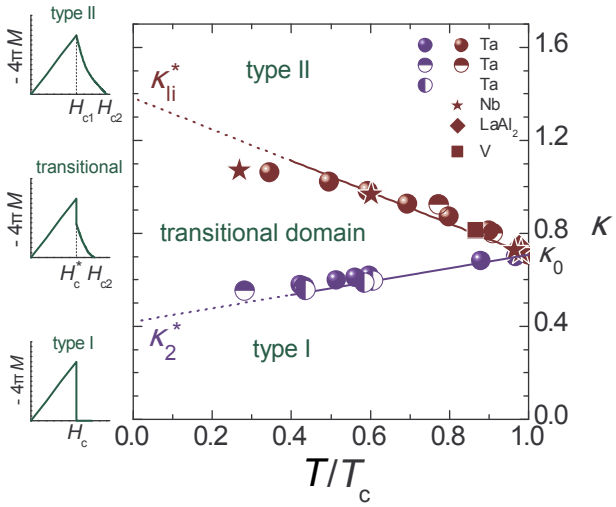

FIG. 2. (Color online) Boundaries of the transitional (inter-type) domain for single-band superconductors. The upper and lower lines represent κ^*_{li} and κ^*_2, given by Eqs. (30) and (31), respectively. Symbols show the collection of different experimental data reported in Ref. 10 and extracted from the qualitative changes of the magnetization curve $M(H)$, see the illustrative sketches given in the three small left panels.

D. Transitional domain: outer boundaries

Mutual deviations of the critical parameters at $T < T_c$ introduce the transitional domain between types I and II in the (κ, T)-plane. Its boundaries are defined by the maximal and minimal critical parameters. Equations (29) - (31) give the transitional interval as $[\kappa_2^*, \kappa_{li}^*]$.

These boundaries can be extracted from the magnetization measured for different κ[10] (see also the review in Ref. 17). In experiments changing κ was achieved in led alloys by varying a thallium content and in TaN samples by nitrogen doping, while remaining in the nearly clean regime. Reported changes of the field dependence of the magnetization $M(H)$ are schematically illustrated

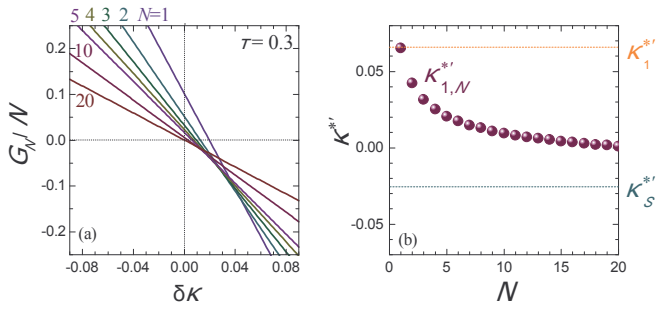

FIG. 3. (Color online) Left panel: the Gibbs free-energy difference for an isolated N-quantum vortex normalized by N versus the deviation of the GL parameter $\delta\kappa = \kappa - \kappa_0$ at $T = 0.7T_c$ and $H = H_c$. Right panel: the derivative $d\kappa^*_{1,N}/d\tau$ as a function of the number of the flux quanta N. Dotted lines display the τ-derivatives of κ^*_1 and κ^*_s.

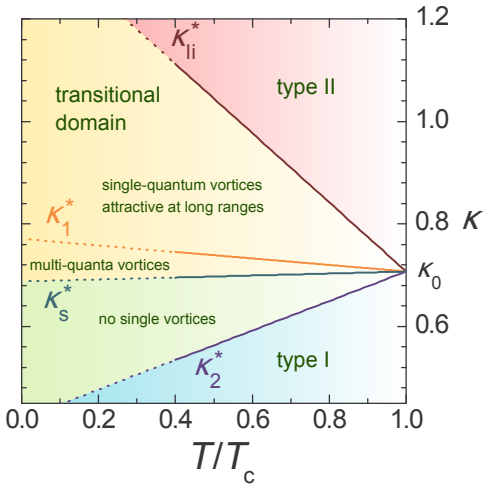

FIG. 4. (Color online) Internal structure of the transitional (inter-type) domain $[\kappa^*_2(T), \kappa^*_{li}(T)]$ as following from analysis of different isolated-vortex solutions. The subdivision in the three subdomains is dictated by the presence of critical parameters $\kappa^*_{1,N}(T)$ displaying stability of N-quantum vortices in the interval $[\kappa^*_s(T), \kappa^*_1(T)]$.

in the left panels in Fig. 2. Inside the transitional domain $M(H)$ has a jump at H^*_c and a non-zero tail at larger fields $H^*_c < H < H_{c2}$. The tail disappears at $\kappa < \kappa^*_2$ and the magnetization acquires the standard type-I appearance. At $\kappa > \kappa^*_{li}$, the jump in the magnetization is absent as expected for type II. Such a magnetization pattern is referred to as type-II/1 in the literature and the related explanations are usually reduced to the long-range attraction between Abrikosov vortices,[17] which is true only to some extent and ignores other important aspects of the inter-type superconductivity (see the next subsection).

The critical parameters κ^*_2 and κ^*_{li}, obtained for different materials, are shown in Fig. 2 together with theoretical results given by Eqs. (30) and (31). One sees that at $T/T_c \gtrsim 0.4$ all experimental data for both κ^*_2 and κ^*_{li} are almost linearly dependent on T/T_c in excellent agreement with the EGL theory, which can be regarded as a further confirmation of its accuracy (see Fig. 1).

E. Transitional domain: internal structure

As noted above, the physics of the transitional domain is commonly restricted to the long-range vortex-vortex attraction. This, however, contradicts to the observation that other critical parameters exist inside this domain with the corresponding changes of admissible inter-type flux patterns. Moreover, the number of such internal critical parameters is infinite due to the infinite degeneracy of the Bogomolnyi point. A comprehensive study of all possible flux configurations and the corresponding subdomains is beyond the scope of this work. However, as an illustration we consider a simple example of the states that generate an infinite set of the critical parameters, namely, vortices that carry an arbitrary number $N \geq 1$ of elementary magnetic-flux quanta (*multi-quantum* or *giant* vortices). Such vortices are known to be unstable in type-II superconductors but this changes in the inter-type regime.

The procedure of solving the GL equations at the Bogomolnyi point for an isolated vortex with an arbitrary N is outlined in Appendix C. Using obtained solutions, we calculate the corresponding integrals I and J and then critical parameters $\kappa^*_{1,N}$, that control the appearance of N-quantum vortices, from Eq. (26). The left panel in Fig. 3 shows the Gibbs free energy difference for an isolated N-quantum vortex divided by N in order to see its stability with respect to the decay into smaller vortices.

Figure 3 demonstrates that for large $\delta\kappa > 0$ an Abrikosov vortex ($N = 1$) has the lowest energy, as expected in type II. For large negative $\delta\kappa < 0$ the Gibbs energy difference is positive for any N and, therefore, any isolated vortex is unstable, as expected in type I. However, when $\delta\kappa \sim 0$, isolated vortices with $N > 1$ become stable. For any value of N there is an interval of $\delta\kappa$'s where $\mathfrak{G}_N(\delta\kappa)/N$ has the lowest value among all the other isolated vortex states and, thus, the N-quantum vortex is most stable in this interval. This is further illustrated by the right panel of Fig. 3 which shows the derivative (tangent) $\kappa^{*\prime}_{1,N} = d\kappa^*_{1,N}/d\tau$ as a function of N. This function decreases monotonously from κ^*_1 to κ^*_s. Thus, the appearance of multi-quantum vortex states introduces an infinite set of critical parameters inside the transitional domain, $\kappa^*_s < \cdots < \kappa^*_{1,N} < \cdots < \kappa^*_{1,2} < \kappa^*_1$ ($\kappa^*_{1,1} \equiv \kappa^*_1$), splitting it into an infinite number of subdomains.

In interval $\kappa^*_1 < \kappa < \kappa^*_{li}$ the Meissner state is unstable with respect to the formation of Abrikosov vortices at fields $H > H_{c,1}$ ($H_{c,1} < H_c$). At $\kappa < \kappa^*_1$ an isolated Abrikosov vortex is less stable then the Meissner state. However, for $\kappa^*_{1,2} < \kappa < \kappa^*_1$ a single two-quantum vor-

tex becomes more favorable thermodynamically than the Meissner state at fields $H > H_{c1}^{N=2}$, with $H_{c1}^{N=2} < H_c$ being the lower critical field for the two-quantum vortex. We note that the condition $H_{c1}^{N} = H_c$ defines critical parameter $\kappa_{1,N}^*$. At $\kappa < \kappa_{1,2}^*$ the energy of both single- and two-quantum vortices are higher than that of the Meissner state and thus we arrive at the subdomain where an isolated vortex with $N = 3$ becomes most favorable for $H > H_{c1}^{N=3}$. When κ decreases further towards κ_s^*, the system sequentially passes through subdomains with larger and large N. Finally, at $\kappa < \kappa_s^*$ isolated vortices become unstable for all N and the representation of the mixed state as a set of weakly interacting vortices is not applicable anymore. We note, however, that at $\kappa_2^* < \kappa < \kappa_s^*$ a spatially nonuniform mixed state with a non-zero penetrating magnetic flux is still possible, following that $H_c < H_{c2}$.

Obtained results are illustrated by a sketch in Fig. 4, where three sectors are distinguished: the upper one, where a single Abrikosov vortex represents the only stable variant of an isolated vortex solution, the lower one, where isolated vortices are not possible, and the middle sector, divided into infinitely many parts, where multi-quantum vortices can exist.

It should be noted that some properties of the mixed state remain degenerate even at $T < T_c$, at least in this order of the τ-expansion. For example, critical parameter $\kappa_{li,N}^*$ that corresponds to changing the sign of the long-range interaction between two N-quantum vortices has the same value κ_{li}^* for all N (see also the last paper in Ref. 11).

We stress again that this analysis of the subdomain structure based on the consideration of isolated multi-quantum vortices is only an illustration. It is, however, sufficient to highlight inadequacy of the assumption that the physics of the magnetic inter-type response is reduced to the single property of the long-range attraction between single-quantum (Abrikosov) vortices.

III. MULTI-BAND SUPERCONDUCTORS

A. GL theory of multi-band materials

Before extending the consideration to multi-band superconductors, we have to make sure that the Bogomolnyi point does exist here. In fact, its existence follows from the microscopic derivation of the GL theory for multi-band materials[19,20,30,31] for the most common case when they do not possess some additional symmetry between contributing bands. Then superconductivity is described by a single-component order parameter Ψ, that determines all the band-gap functions in the lowest order in τ as

$$\overrightarrow{\Delta}^{(0)} = \Psi \overrightarrow{\xi}, \tag{32}$$

where $\overrightarrow{\Delta}^{(0)} = (\Delta_1^{(0)}, \dots, \Delta_M^{(0)})^T$ is the vector of the band-gap components, M is the total number of bands, and $\overrightarrow{\xi}$ is an eigenvector of a matrix that controls the equation for T_c (referred to as the linearized gap equation).[20,30] If a system possesses additional symmetry between the carrier bands, several such eigenvectors may exist, which is defined by the dimensionality of the irreducible representation of the symmetry group.[22,23] Thus, what determines the number of the order-parameter components is the dimensionality of the representation and not the number of the contributing bands. When no such additional symmetry exists, a solution of the linearized gap equation is not degenerate and the system has a single order parameter associated with the single eigenvector of the matrix in the linearized gap equation.[30]

This order parameter satisfies the standard single-component GL equation

$$a\,\Psi + b\,|\Psi|^2\Psi - \mathcal{K}\,\mathfrak{D}^2\Psi = 0, \tag{33}$$

however, its coefficients incorporate contributions of all bands

$$a = \sum_n \xi_n^2 a_n, \quad b = \sum_n \xi_n^4 b_n, \quad \mathcal{K} = \sum_n \xi_n^2 \mathcal{K}_n, \tag{34}$$

where a_n, b_n and $\mathcal{K}_n$ are obtained for band n. If considering the clean limit and spherical Fermi surfaces for each band, these coefficients are given by Eq. (10) with the band density of states $N_n(0)$ and band Fermi velocity v_{Fn}.

The fact that the GL theory is single-component means that all conclusions of this theory for single-band superconductors hold in the multi-band case as well. In particular, multi-band superconductors follow the standard picture of two superconductivity types separated by the infinitely degenerate Bogomolnyi point. One can also expect that at $T < T_c$ the degeneracy is lifted, giving rise to the inter-type superconductivity in a finite transitional interval (domain) of κ's. However, in order to confirm this, one needs to go beyond the standard GL theory, now with the account of the multi-band structure.

B. Gibbs free energy difference

As in the single-band case, we start with Eqs. (1) and (2). However, now the Gibbs free-energy difference $\mathfrak{G}$ must be calculated using the EGL formalism for multi-band superconductors.[20] Although the EGL approach applies, in principle, to an arbitrary number of bands, here we restrict our analysis to two-band systems, where most of pertinent quantities can be obtained in the explicit analytical form.

As before, $\mathfrak{G}$ is calculated by means of the perturbation expansion over τ, which is achieved by expanding all relevant physical quantities. In particular, the vector gap function writes as

$$\overrightarrow{\Delta} = \tau^{1/2}\Big(\overrightarrow{\Delta}^{(0)} + \tau\overrightarrow{\Delta}^{(1)} + \tau^2\overrightarrow{\Delta}^{(2)} \dots\Big), \tag{35}$$

where $\overrightarrow{\Delta}^{(0)}$ is given by Eq. (32), while $\overrightarrow{\Delta}^{(1)}$ and $\overrightarrow{\Delta}^{(2)}$ are corrections in the next two orders in τ. The τ-expansion for the magnetic field is given by Eq. (3). The free-energy density is obtained as[20]

$$\mathfrak{f} = \tau^2\big(\tau^{-1}\mathfrak{f}^{(-1)} + \mathfrak{f}^{(0)} + \tau\mathfrak{f}^{(1)} + \dots\big), \tag{36}$$

where the lowest-order contribution reads

$$\mathfrak{f}^{(-1)} = \big\langle \overrightarrow{\Delta}^{(0)}\big|\check{L}\big|\overrightarrow{\Delta}^{(0)}\big\rangle, \tag{37}$$

with $\langle\cdots\rangle$ denoting the scalar product of vectors in the band space. Here $\check{L}$ for a two-band system is given by

$$\check{L} = \frac{1}{G}\begin{pmatrix} g_{22} - GN_1(0)\mathcal{A} & -g_{12} \\ -g_{12} & g_{11} - GN_2(0)\mathcal{A}\end{pmatrix}, \tag{38}$$

where $g_{nm} = g_{mn}$ are the coupling constants (assumed real), $G = g_{11}g_{22} - g_{12}^2$, and

$$\mathcal{A} = \ln\left(\frac{2e^{\gamma}\hbar\omega_c}{\pi T_c}\right), \tag{39}$$

with ω_c the cut-off frequency. At the stationary point the contribution $\mathfrak{f}^{(-1)}$ disappear due to the (linearized gap) equation

$$\check{L}\overrightarrow{\Delta}^{(0)} = 0, \tag{40}$$

which determines T_c and the eigenvector $\overrightarrow{\xi}$. The next-order contribution to the free energy density is the GL functional

$$\begin{aligned}\mathfrak{f}^{(0)} =& \frac{\mathfrak{B}^2}{8\pi} + \Big(\big\langle\overrightarrow{\Delta}^{(0)}\big|\check{L}\big|\overrightarrow{\Delta}^{(1)}\big\rangle + \text{c.c.}\Big) \\ &+ \sum_n\Big[a_n|\Delta_n^{(0)}|^2 + \frac{b_n}{2}|\Delta_n^{(0)}|^4 + \mathcal{K}_n\big|\mathfrak{D}\,\Delta_n^{(0)}\big|^2\Big].\end{aligned} \tag{41}$$

The leading correction to the GL functional is obtained in the form

$$\begin{aligned}\mathfrak{f}^{(1)} =& \frac{(\mathfrak{B}\cdot\mathfrak{b})}{4\pi} + \Big(\big\langle\overrightarrow{\Delta}^{(0)}\big|\check{L}\big|\overrightarrow{\Delta}^{(2)}\big\rangle + \text{c.c.}\Big) \\ &+ \big\langle\overrightarrow{\Delta}^{(1)}\big|\check{L}\big|\overrightarrow{\Delta}^{(1)}\big\rangle + \sum_n \mathfrak{f}_n^{(1)}.\end{aligned} \tag{42}$$

As in the single-band case it is convenient to split the band-dependent quantities $\mathfrak{f}_n^{(1)}$ into two parts

$$\mathfrak{f}_n^{(1)} = \mathfrak{f}_{n,1}^{(1)} + \mathfrak{f}_{n,2}^{(1)}, \tag{43}$$

where $\mathfrak{f}_{n,1}^{(1)}$ contains only the lowest order contributions to the band gap and the magnetic field

$$\begin{aligned}\mathfrak{f}_{n,1}^{(1)} =& \frac{a_n}{2}|\Delta_n^{(0)}|^2 + 2\,\mathcal{K}_n\big|\mathfrak{D}\Delta_n^{(0)}\big|^2 + \frac{b_n}{36}\,\frac{e^2\hbar^2}{m^2\mathbb{c}^2}\,\mathfrak{B}^2\big|\Delta_n^{(0)}\big|^2 \\ &+ b_n|\Delta_n^{(0)}|^4 - \mathcal{Q}_n\Big\{\big|\mathfrak{D}^2\Delta_n^{(0)}\big|^2 + \frac{1}{3}\big(\mathrm{rot}\,\mathfrak{B}\cdot\mathbf{i}_n\big) \\ &+ \frac{4e^2}{\hbar^2\mathbb{c}^2}\,\mathfrak{B}^2\big|\Delta_n^{(0)}\big|^2\Big\} - \frac{\mathcal{L}_n}{2}\Big\{8\,|\Delta_n^{(0)}|^2\big|\mathfrak{D}\Delta_n^{(0)}\big|^2 \\ &+ \big[\Delta_n^{(0)2}(\mathfrak{D}^*\Delta_n^{(0)*})^2 + \text{c.c.}\big]\Big\} - \frac{c_n}{3}\big|\Delta_n^{(0)}\big|^6,\end{aligned} \tag{44}$$

while $\mathfrak{f}_{n,2}^{(1)}$ includes also the leading corrections to the band gap and the field

$$\begin{aligned}\mathfrak{f}_{n,2}^{(1)} =& \big(a_n + b_n\big|\Delta_n^{(0)}\big|^2\big)\big(\Delta_n^{(0)*}\Delta_n^{(1)} + \text{c.c.}\big) \\ &+ \mathcal{K}_n\Big[\big(\mathfrak{D}\Delta_n^{(0)}\cdot\mathfrak{D}^*\Delta_n^{(1)*} + \text{c.c.}\big) - \big(\mathfrak{a}\cdot\mathbf{i}_n\big)\Big].\end{aligned} \tag{45}$$

Here we use the notation

$$\mathbf{i}_n = \mathbb{i}\,\frac{2e}{\hbar\,\mathbb{c}}\big(\Delta_n^{(0)}\mathfrak{D}^*\Delta_n^{(0)*} - \Delta_n^{(0)*}\,\mathfrak{D}\Delta_n^{(0)}\big), \tag{46}$$

and coefficients $\mathcal{Q}_n$, $\mathcal{L}_n$ and c_n are calculated for each band separately, similarly to a_n, b_n and $\mathcal{K}_n$ discussed above.

The obtained free energy functional contains additional terms that are not present in the single-band case. One extra contribution is found in Eq. (41) mixing $\overrightarrow{\Delta}^{(0)}$ with $\overrightarrow{\Delta}^{(1)}$. Equation (42) includes two more such terms: one mixes $\overrightarrow{\Delta}^{(0)}$ with $\overrightarrow{\Delta}^{(2)}$ and the other reads $\langle\overrightarrow{\Delta}^{(1)}|\check{L}|\overrightarrow{\Delta}^{(1)}\rangle$. However, both mixing contributions are zero by virtue of Eq. (40). The last of the extra terms does not disappear, $\langle\overrightarrow{\Delta}^{(1)}|\check{L}|\overrightarrow{\Delta}^{(1)}\rangle \neq 0$. Nevertheless, it can be calculated explicitly without solving equations for $\overrightarrow{\Delta}^{(1)}$. In order to do this we write the leading correction to the gap as the expansion

$$\overrightarrow{\Delta}^{(1)} = \psi\,\overrightarrow{\xi} + \phi\,\overrightarrow{\eta}, \tag{47}$$

where $\overrightarrow{\eta}$ and $\overrightarrow{\xi}$ must be linearly independent. Using Eqs. (32), (40), and (47), one finds

$$\langle\overrightarrow{\Delta}^{(1)}|\check{L}|\overrightarrow{\Delta}^{(1)}\rangle = |\phi|^2\,\langle\overrightarrow{\eta}|\check{L}|\overrightarrow{\eta}\rangle. \tag{48}$$

where ϕ is related to Ψ by a simple algebraic expression[20]

$$\phi = -\frac{G}{4g_{12}}\big(\alpha\Psi + \beta\Psi\big|\Psi\big|^2 + \Gamma\mathfrak{D}^2\Psi\big), \tag{49}$$

with

$$\alpha = \sum_n \xi_n\eta_n a_n,\ \beta = \sum_n \xi_n^3\eta_n b_n,\ \Gamma = \sum_n \xi_n\eta_n\mathcal{K}_n. \tag{50}$$

It remains to note that a sum of $(\mathfrak{B}\cdot\mathfrak{b})/(4\pi)$ and $\sum_n f_{n,2}^{(1)}$ disappears as previously in the single-band case. Thus, in order to calculate $\mathfrak{G}$ in the two lowest non-vanishing orders, we need only to know solutions Ψ and $\mathfrak{B}$ ($\mathfrak{A}$) to the GL equation (33).

For two contributing bands the eigenvalue problem for the matrix $\check{L}$ is solved analytically and the eigenvector can be chosen as $\overrightarrow{\xi}^T = (S^{-1/2}, S^{1/2})$, where

$$S = \frac{1}{2\lambda_{12}}\Big[\lambda_{22} - \frac{\lambda_{11}}{\eta} + \sqrt{\Big(\lambda_{22} - \frac{\lambda_{11}}{\eta}\Big)^2 + 4\frac{\lambda_{12}^2}{\eta}}\Big], \tag{51}$$

with the dimensionless coupling constant $\lambda_{nm} = g_{nm}N(0)$, $N(0) = \sum_i N_i(0)$, and $\eta = N_2(0)/N_1(0)$. The other vector in the expansion (47) is chosen as

$\overrightarrow{\eta}^T = (S^{-1/2}, -S^{1/2})$. Then the coefficients that appear in the final expression for the free energy density are given by

$$
\begin{aligned}
&a = \frac{a_1}{S} + S a_2, \quad b = \frac{b_1}{S^2} + S^2 b_2, \quad \mathcal{K} = \frac{\mathcal{K}_1}{S} + S\mathcal{K}_2,\\
&\alpha = \frac{a_1}{S} - S a_2, \quad \beta = \frac{b_1}{S^2} - S^2 b_2, \quad \mathit{\Gamma} = \frac{\mathcal{K}_1}{S} - S\mathcal{K}_2,\\
&c = \frac{c_1}{S^3} + S^3 c_2, \quad \mathcal{Q} = \frac{\mathcal{Q}_1}{S} + S\mathcal{Q}_2, \quad \mathcal{L} = \frac{\mathcal{L}_1}{S^2} + S^2\mathcal{L}_2,\\
&\bar{c} = \frac{ca}{3b^2}, \quad \bar{\mathcal{Q}} = \frac{\mathcal{Q}a}{\mathcal{K}^2}, \quad \bar{\mathcal{L}} = \frac{\mathcal{L}a}{b\mathcal{K}}, \quad \bar{G} = \frac{Ga}{4g_{12}},\\
&\bar{\alpha} = \frac{\alpha}{a} - \frac{\mathit{\Gamma}}{\mathcal{K}}, \quad \bar{\beta} = \frac{\beta}{b} - \frac{\mathit{\Gamma}}{\mathcal{K}}.
\end{aligned}
\tag{52}
$$

One more quantity needed to calculate the Gibbs free-energy difference in Eqs. (1) and (2) is the thermodynamic critical field H_c. Its expression differs from the single-band case. While its τ-expansion is still given by Eq. (13), with $H_c^{(0)}$ defined by Eq. (14) and constants a and b taken from Eq. (52), its leading correction $H_c^{(1)}$ has additional contributions, i.e.,

$$
H_c^{(1)} = H_c^{(0)}\Big[-\frac{1}{2} - \bar{c} - \bar{G}(\bar{\alpha} - \bar{\beta})^2\Big]. \tag{53}
$$

In the following we also employ the dimensionless quantities introduced by Eqs. (15) and (16), with the difference that the coefficients are now defined by Eq. (52).

The τ-expansion of the Gibbs free energy difference is defined by Eq. (17), with $\mathfrak{g}^{(0)}$ given by Eq. (18) (with multi-band coefficients) and with the leading correction

$$
\begin{aligned}
\mathfrak{g}^{(1)} =& \left(\frac{\mathfrak{B}}{\kappa\sqrt{2}} - 1\right)\left[\frac{1}{2} + \bar{c} + \bar{G}\big(\bar{\alpha} - \bar{\beta}\big)^2\right] + \frac{1}{\kappa^2}\left|\mathfrak{D}\Psi\right|^2\\
&- \frac{1}{2}\left|\Psi\right|^2 + \left|\Psi\right|^4 + \bar{c}\left|\Psi\right|^6 + \bar{G}|\Psi|^2\left(\bar{\alpha} - \bar{\beta}|\Psi|^2\right)^2\\
&+ \frac{\bar{\mathcal{Q}}}{4\kappa^4}\Big\{\left|\mathfrak{D}^2\Psi\right|^2 + \frac{1}{3}(\mathrm{rot}\,\mathfrak{B})^2 + \mathfrak{B}^2|\Psi|^2\Big\}\\
&+ \frac{\bar{\mathcal{L}}}{4\kappa^2}\Big\{8\left|\Psi\right|^2\left|\mathfrak{D}\Psi\right|^2 + \left[\Psi^2(\mathfrak{D}^*\Psi^*)^2 + \mathrm{c.c.}\right]\Big\}.
\end{aligned}
\tag{54}
$$

As in the single-band case we employ the expansion with respect to $\delta\kappa = \kappa - \kappa_0$ and finally, in the lowest and next orders in τ, obtain

$$
\begin{aligned}
\mathfrak{G} =& \tau^2\Big\{ -\sqrt{2}\mathcal{I}\delta\kappa + \tau\Big[\Big(1 - \bar{c} + 2\bar{\mathcal{Q}} + \bar{G}\,\bar{\beta}\\
&\times\big(2\bar{\alpha} - \bar{\beta}\big)\Big)\mathcal{I} + \Big(2\bar{\mathcal{L}} - \bar{c} - \frac{5}{3}\bar{\mathcal{Q}} - \bar{G}\bar{\beta}^2\Big)\mathcal{J}\Big]\Big\},
\end{aligned}
\tag{55}
$$

where $\mathcal{I}$ and $\mathcal{J}$ are as previously given by Eq. (25). One notes that in the dimensionless units solutions of the GL theory for both single- and two-band systems are the same, which is a significant advantage of the EGL formalism.

Equation (55) differs from its single-band counterpart (24) in two respects. First, the coefficients $\bar{c}$, $\bar{\mathcal{L}}$ and $\bar{\mathcal{Q}}$ comprise contributions of two bands and so are different from $\tilde{c}$, $\tilde{\mathcal{L}}$ and $\tilde{\mathcal{Q}}$. Second, there are extra terms $\propto \bar{G}$ which are related to the difference between the spatial profiles of the band gap functions Δ_n[20] and, thus, to the interplay of different band characteristic lengths.

C. Critical parameters

Using $\mathfrak{G}$ of Eq. (55), we resolve Eq. (2) and obtain the general expression for critical parameter κ^* in the two-band case as

$$
\begin{aligned}
\kappa^* =& \kappa_0\Big\{1 + \tau\Big[1 - \bar{c} + 2\bar{\mathcal{Q}} + \bar{G}\bar{\beta}\big(2\bar{\alpha} - \bar{\beta}\big)\\
&+ \frac{\mathcal{J}}{\mathcal{I}}\Big(2\bar{\mathcal{L}} - \bar{c} - \frac{5}{3}\bar{\mathcal{Q}} - \bar{G}\bar{\beta}^2\Big)\Big]\Big\}.
\end{aligned}
\tag{56}
$$

Similarly to Eq. (26) this expression is generally related to any non-uniform flux configuration and thus defines the inter-type domain with all its subdomains in the two-band case. However, the parameters entering Eq. (56) are not reduced to universal numbers any more but read as

$$
\begin{aligned}
\bar{c} =& \tilde{c}\,\frac{\big(1 + \eta S^6\big)\big(1 + \eta S^2\big)}{\big(1 + \eta S^4\big)^2},\\
\bar{\mathcal{Q}} =& \tilde{Q}\,\frac{\big(1 + \eta\gamma^4 S^2\big)\big(1 + \eta S^2\big)}{\big(1 + \eta\gamma^2 S^2\big)^2},\\
\bar{\mathcal{L}} =& \tilde{\mathcal{L}}\,\frac{\big(1 + \eta\gamma^2 S^4\big)\big(1 + \eta S^2\big)}{\big(1 + \eta\gamma^2 S^2\big)\big(1 + \eta S^4\big)},\\
\bar{\alpha} =& \frac{1 - \eta S^2}{1 + \eta S^2} - \frac{1 - \eta\gamma^2 S^2}{1 + \eta\gamma^2 S^2},\\
\bar{\beta} =& \frac{1 - \eta S^4}{1 + \eta S^4} - \frac{1 - \eta\gamma^2 S^2}{1 + \eta\gamma^2 S^2},\\
\bar{G} =& -\frac{\lambda_{11}\lambda_{22} - \lambda_{12}^2}{4\,\lambda_{12}\,S}\frac{1 + \eta S^2}{1 + \eta},
\end{aligned}
\tag{57}
$$

where $\gamma = v_{F,2}/v_{F,1}$ is the ratio of the band Fermi velocities, and $\tilde{c}$, $\tilde{\mathcal{Q}}$ and $\tilde{\mathcal{L}}$ are given by Eq. (20). One sees that κ^* in Eq. (56) depends on five microscopic parameters: three dimensionless coupling constants λ_{11}, λ_{22} and λ_{12}, the ratio of the band DOS's η and the ratio of the band Fermi velocities γ.

D. Transitional domain

The transitional domain is defined in the multi-band case by the same criteria of the type interchange. In particular, we consider the critical parameters κ_{li}^*, κ_1^*, κ_s^*, κ_2^* as well as $\kappa_{1,N}^*$ related to multi-quantum vortices. The corresponding solutions of the dimensionless GL equations are adopted from the single-band theory.

To calculate coefficients (57) we use material parameters of several prototype systems: MgB_2,[32] OsB_2,[33]

	λ_{11}	λ_{22}	λ_{12}	η
MgB_2[32]	2.41	0.78	0.37	1.37
OsB_2[33]	0.39	0.29	0.0084	1.22
$FeSe_{0.94}$[34]	0.48	0.39	0.005	≈ 1
LiFeAs[35]	0.63	0.64	0.008	≈ 1

TABLE II. Microscopic material parameters used in our calculations.

$FeSe_{0.94}$,[34] and LiFeAs.[35] These parameters are summarized in Table II. Due to lack of experimental data on the band Fermi velocities the ratio $\gamma = v_{F,2}/v_{F,1}$ is assumed to be a free variable. Calculated tangents $d\kappa^*/d\tau$ of parameters κ^*_{li}, κ^*_1, κ^*_s, and κ^*_2 are shown in Fig. 5 as functions of γ. The color scheme in Fig. 5 remains the same as in the sketch of Fig. 4.

One notes that inequality $\kappa^*_2 < \kappa^*_s < \kappa^*_1 < \kappa^*_{li}$, that specifies the internal structure of the inter-type domain, holds for all considered parameters, so that the curves do not intersect. In particular, the outer boundaries of the domain are given by κ^*_2 and κ^*_{li}. Thus, for the chosen parameters the inter-type regimes in single- and two-band superconductors are qualitatively similar and therefore many conclusions drawn from the analysis of the single-band case apply also for two-band (multi-band) superconductors.

However, Fig. 5 demonstrates a systematic enlargement of the inter-type region in two-band systems, and this enlargement becomes most notable when the discrepancy between band Fermi velocities increases. Outer boundaries κ^*_2 and κ^*_{li} shift in the opposite directions, so that the difference $\kappa^*_{li} - \kappa^*_2$ grows when γ increases. In panel (d) this difference is also increased in the opposite limit $\gamma \ll 1$. The internal subdomains widens accordingly.

The enlargement magnitude can be extraordinary large. For example, it is more than an order of magnitude at $\gamma = 6$ for parameters of MgB_2 (a), OsB_2 (b), and $FeSe_{0.94}$ (c). To have an idea about how large can be γ, we remark that according to first-priciple calculations,[36] the band Fermi velocities in the c-axis direction for MgB_2 are estimated as $7 \times 10^4\, m/s$ (band 1, σ) and $6 \times 10^5\, m/s$ (band 2, π), which gives $\gamma \approx 9$. The universality of the enlargement and its magnitude make it possible to expect that many multi-band superconductors can enter the inter-type regime when the temperature is lowered.

One can further demonstrate that the observed enlargement of the inter-type domain is generally related to the competition of different band length-scales. Considering only contributions proportional to $\bar{G}$ in Eq. (56) [as already mentioned after Eq. (55), such terms are responsible for different spatial profiles of band condensates], and taking into account that $\alpha \sim \beta$, the upper boundary

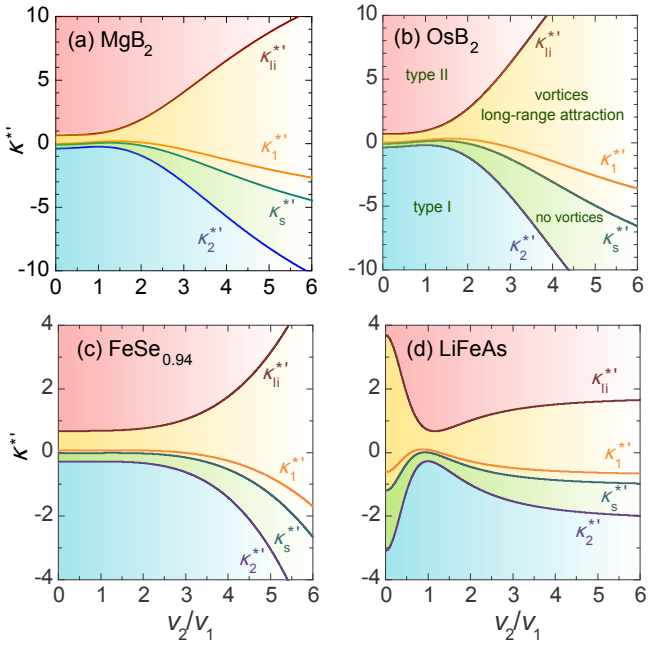

FIG. 5. (Color online) The derivative $\kappa^{*'} = d\kappa^*/d\tau$ as a function of $\gamma = v_{F,2}/v_{F,1}$ for κ^*_{li}, κ^*_1, κ^*_s, and κ^*_2. The results are calculated from Eq. (56) for the material parameters of MgB_2 (a), OsB_2 (b), $FeSe_{0.94}$ (c) and LiFeAs (d).

of the transitional domain is estimated as

$$\frac{d\kappa^*_{li}}{d\tau} \sim -\kappa_0 \bar{G} \bar{\beta}^2 > 0, \tag{58}$$

where we again use $\mathcal{J}/\mathcal{I} = 2$ for the vortex-vortex long-range interaction asymptote. This expression is positive because $\bar{G} < 0$ for the parameters in Tab. II. For the lower boundary one uses $\mathcal{J}/\mathcal{I} = 0$ and obtains

$$\frac{d\kappa^*_2}{d\tau} \sim \kappa_0 \bar{G} \bar{\beta}^2 < 0. \tag{59}$$

This demonstrates that the boundaries of the transitional domain are shifted by an equal value in the opposite directions, which is in a very good agreement with the complete results shown in Fig. 5. Thus, the competition of different band length-scales does not produce a new multi-band type of superconductivity (contrary to the controversial idea of Refs. 1 and 18, see the Introduction) but enhances the inter-type superconducting behavior.

It was mentioned earlier that the inter-type regime in the single-band case is related to non-local interactions that can be described only beyond the GL theory.[17] This non-locality is inherent to the BCS gap equation, which can be demonstrated, for example, by expanding it with respect to the gap parameter. This expansion, which is an intermediate step in deriving the EGL formalism, generates a series of contributions in the form of multiple spatial integrals.[20] The GL theory minimizes this non-locality by keeping only the lowest order derivatives

when applying the gradient expansion to the integrals (this is why the GL theory is often referred to as a weakly-nonlocal approach). In this approximation the transitional domain shrinks to $\kappa = \kappa_0$. The EGL approach incorporates higher-order spatial gradients, which results in a finite interval of κ's (at $T < T_c$) with the inter-type superconducting magnetic response.

The appearance of multiple bands further enhances non-local effects. Indeed, on the mean-field level multi-band superconductors are described by a set of coupled equations for each band-gap function. The fact that the non-locality is enhanced by the inter-band coupling can be easily demonstrated with a simple example of two coupled linear differential equations. Resolving one of them and substituting the result into the other, one obtains additional non-local interactions, often referred to as "memory" effects in the context of dynamical equations. Thus, we again conclude that the enlargement of the transitional domain is a generic property of multi-band superconductors independent of fine details of theoretical models. One can also expect that the effect increases with the number of contributing bands.

IV. CONCLUSIONS

This work investigated how the multi-band structure affects the mixed state and the interchange between superconductivity types. The analysis was done within the EGL formalism that obtains corrections to the GL theory as the perturbation expansion over the proximity to the transitional temperature. An advantage of this approach is that it is applicable to systems with an arbitrary number of bands, which allows one to consider single- and multi-band superconductivity from a single perspective, and that it gives universal analytical expressions for the critical parameters defining the transitional domain.

An important conclusion of the EGL-based analysis is that in the absence of additional symmetry multi-band systems are described by a single-component order parameter. It then follows that superconductivity classification in multi-band systems is qualitatively similar to the single-band case, with types I and II separated by a transitional domain with the inter-type superconducting magnetic response.

Our discussion started with the single-band case for which the concept of the inter-type/transitional domain was introduced and studied by calculating the critical parameters at which the corresponding inhomogeneous flux configuration or its particular property appears/disappears. It was demonstrated that the inter-type domain has a complex structure with different possible variants of the mixed state. This structure appears as a result of the removal of the infinite degeneracy of the Bogomolnyi point when lowering temperature.

As a particular example, we calculated the critical parameters that correspond to an isolated vortex solution with an arbitrary number of the flux quanta. A complete analysis of any other plausible flux configuration can also be done within the EGL formalism but this general consideration is beyond the scope of the current work. However, the obtained hierarchy of the critical parameters demonstrates that the long-range attraction between Abrikosov vortices does not suffice to explain the inter-type physics.

We generalized our consideration to the multi-band case and investigated a two-band prototype allowing for explicit analytical results. Following the structure of the EGL formalism, one concludes that the qualitative results of this work apply to systems with an arbitrary number of bands. A more elaborate analysis of the general multi-band case will be presented elsewhere.

A central result of this work is that the inter-type domain extends in multi-band superconductors. The enlargement is a generic phenomenon and independent of the details of the model for band states. Its origin is the non-locality of interactions in the aggregate condensate due to the appearance of multiple bands. The enlargement becomes huge when the band microscopic parameters, e.g., the band Fermi velocities, are significantly different. Our results make it possible to expect that many of multi-band superconductors, especially with large disparity between bands, are in fact in the transitional domain. One of the candidates is MgB_2 which can enter the inter-type regime at lowered temperatures, which can be an explanation of its non-standard vortex configurations.[1] However, a more detailed analysis accounting for anisotropy of its bands is certainly required.

Finally, we note that the size and structure of the inter-type domain in the (κ, T)-plane may be rather sensitive to many other physical aspects, such as disorder, band dimensionality, as well as the presence of shallow bands, where contributing electrons have almost zero velocities.[37]

ACKNOWLEDGMENTS

This work was supported by Brazilian agencies CNPq (grants 307552/2012-8 and 141911/2012-3) and FACEPE (APQ-0589-1.05/08) as well as by the U.S. Department of Energy, Office of Science, Materials Sciences and Engineering Division.

Appendix A: Bogomolnyi equations and topological degeneracy of the GL theory

Here it is shown that at $\kappa = \kappa_0$ the GL equations are reduced to a couple of first-order equations referred to as the Bogomolnyi self-duality equations[5,6] and also known in the literature as the Sarma solution.[3] The derivation of the Bogomolnyi equations follows the standard procedure (see, e.g., the remark about the Sarma solution in Ref. 3) and is presented here for the convenience of the reader.

Our starting point is the standard GL equations

$$a\,\Psi + b\,|\Psi|^2\Psi - \mathcal{K}\,\boldsymbol{\mathfrak{D}}^2\Psi = 0, \quad \frac{1}{4\pi}\mathrm{rot}\,\boldsymbol{\mathfrak{B}} = \mathcal{K}\mathbf{i}, \quad \text{(A1)}$$

where $\mathbf{i}$ is given by Eq. (9) [for both the single- and two-band cases]. A magnetic field is set along the z axis, $\boldsymbol{\mathfrak{B}} = (0, 0, \mathcal{B})$, so that the system is homogeneous along this axis and the order parameter is independent of z. We introduce the new gauge invariant gradients

$$\mathfrak{D}_\pm = \mathfrak{D}_x \pm \mathbb{i}\mathfrak{D}_y, \quad \text{(A2)}$$

that satisfy the identity

$$\boldsymbol{\mathfrak{D}}^2 = \mathfrak{D}_+\mathfrak{D}_- + \frac{2\,e}{\hbar\,\mathbb{c}}\,\mathcal{B}. \quad \text{(A3)}$$

Let us assume that a solution to the GL formalism satisfies the first-order equation

$$\mathfrak{D}_-\Psi = 0, \quad \text{(A4)}$$

i.e., the first of the two Bogomolnyi equations. Now we proceed to establish the condition under which this assumption is correct. One immediately notices that when inserting Eq. (A3) in Eq. (A1), the latter simplifies to

$$|\Psi|^2 = -\frac{1}{b}\Big(a - \frac{2\,e\mathcal{K}}{\hbar\,\mathbb{c}}\mathcal{B}\Big), \quad \text{(A5)}$$

which is known as the second Bogomolnyi equation. As seen, Eqs. (A4) and (A5) dictate that the first equation in the GL set (A1) is satisfied.

Now we turn to the second GL equation, that represents the Ampére law, and check its compatibility with Eqs. (A4) and (A5). Taking into account that $\mathrm{rot}\,\boldsymbol{\mathfrak{B}} = (\partial_y\mathcal{B}, -\partial_x\mathcal{B}, 0)$, one can find from the second GL equation that

$$\frac{1}{4\pi}\big(\partial_y + \mathbb{i}\partial_x\big)\mathcal{B} = \mathbb{i}\,\frac{2e\mathcal{K}}{\hbar\,\mathbb{c}}\Psi\mathfrak{D}_+^*\Psi^*. \quad \text{(A6)}$$

The left-hand-side of this equation can be also calculated by using Eq. (A5). This yields

$$\frac{1}{4\pi}\big(\partial_y + \mathbb{i}\partial_x\big)\mathcal{B} = \frac{\hbar\mathbb{c}b}{8\pi e\mathcal{K}}\Big[\Psi\big(\partial_y + \mathbb{i}\partial_x\big)\Psi^* + \Psi^*\big(\partial_y + \mathbb{i}\partial_x\big)\Psi\Big]. \quad \text{(A7)}$$

Substituting the explicit form of the first Bogomolnyi equation

$$\big(\partial_y + \mathbb{i}\partial_x\big)\Psi = \frac{2\,e}{\hbar\mathbb{c}}\big(\mathbb{i}\mathfrak{A}_y - \mathfrak{A}_x\big)\Psi \quad \text{(A8)}$$

into Eq. (A7), one obtains the latter in the form

$$\frac{1}{4\pi}\big(\partial_y + \mathbb{i}\partial_x\big)\mathcal{B} = \mathbb{i}\,\frac{\hbar\,\mathbb{c}b}{8\pi e\mathcal{K}}\,\Psi\mathfrak{D}_+^*\Psi^*. \quad \text{(A9)}$$

Comparing Eq. (A9) with the second GL equation in Eq. (A6), one finds the following consistency condition:

$$\frac{2e\mathcal{K}}{\hbar\,\mathbb{c}} = \frac{\hbar\,\mathbb{c}b}{8\pi e\mathcal{K}}. \quad \text{(A10)}$$

Now, using the definition of the GL parameter κ which is written as

$$\kappa^2 = \frac{\lambda_L^2}{\xi^2} = \frac{\hbar^2\mathbb{c}^2 b}{32e^2\pi\mathcal{K}^2}, \quad \text{(A11)}$$

we find from Eq. (A10)

$$\kappa = \kappa_0 \equiv \frac{1}{\sqrt{2}}. \quad \text{(A12)}$$

Thus, solutions to the GL formalism Ψ and $\boldsymbol{\mathfrak{A}}(\boldsymbol{\mathfrak{B}})$ obey the two Bogomolnyi self-duality equations at $\kappa = \kappa_0$.

When utilizing the dimensionless units of Eq. (15), the Bogomolnyi equations are reduced to (we omit tildes, as previously)

$$\big(\partial_y + \mathbb{i}\partial_x\big)\Psi = \big(\mathfrak{A}_x - \mathbb{i}\mathfrak{A}_y\big)\Psi, \quad \text{(A13)}$$

$$\mathcal{B} = 1 - |\Psi|^2. \quad \text{(A14)}$$

Substituting these relations into Eq. (18), for the GL contribution to the Gibbs free energy one obtains (at $\kappa = \kappa_0$)

$$\mathfrak{G}^{(0)} = \int \mathfrak{g}^{(0)} d\mathbf{r} = 0, \quad \text{(A15)}$$

which holds for an arbitrary solution to the GL formalism, irrespective of its topological configuration.

Appendix B: Superconducting-normal interface and isolated single- and multi-quantum vortices

Equations (A13) and (A14) can be used to find a solution to the GL equations for any desired topological configuration of the mixed state at $\kappa = \kappa_0$. Examples of this can be found in earlier works, see, e.g., 15. Since, however, most of them provided only sketchy details, here we outline the main solving steps for the convenience of the reader. Here we consider solutions to the Bogomolnyi equations for the normal-superconducting interface (flat domain wall) and also for isolated single- and multi-quantum vortices.

First we outline how to obtain a solution for a flat interface (domain wall) between the superconducting and normal state that arises in the problem of the surface energy. The domain wall is chosen to be parallel to the (y, z)-plane, so that all observables vary only along the x-axis. We choose the vector potential as $\boldsymbol{\mathfrak{A}} = (0, \mathcal{A}, 0)$ and then recast the first Bogomolnyi equation (A13) in the form

$$\Psi' = -\mathcal{A}\,\Psi, \quad \text{(B1)}$$

where prime denotes the derivative with respect to x. The second Bogomolnyi equation (A14) now reads

$$\mathcal{A}' = 1 - \Psi^2, \tag{B2}$$

where Ψ is real because the GL equations do not involve any imaginary coefficients in the chosen gauge. Differentiating this equation and using Eq. (B1), one obtains the equation

$$\mathcal{A}'' = 2\mathcal{A}(1 - \mathcal{A}'). \tag{B3}$$

It differs from the equation for the vector potential for the superconducting-normal interface problem in Refs. 3 and 4 only by the presence of factor 2 (due to different dimensionless units in our work). This equation must be solved with the boundary conditions that follows from that the system is in the superconducting states to, say, the left of the wall and, respectively, normal to its right. The boundary conditions read

$$\mathcal{A}(x \to -\infty) = 0, \quad \mathcal{A}'(x \to +\infty) = 1, \tag{B4}$$

so that the magnetic field approaches zero in the superconducting domain while goes to the thermodynamic critical field $\mathcal{B} = 1$ in the normal domain.

Isolated vortex solutions are naturally considered in the cylindrical coordinates (ρ, θ, z). The solution for a vortex with the single magnetic flux quantum is sought in the form

$$\Psi = \Phi(\rho)\exp(-\mathrm{i}\theta) = (x - \mathrm{i}y)\frac{\Phi(\rho)}{\rho}, \tag{B5}$$

where Φ is a real function. The vector potential is chosen so that it has only single θ-component, $\mathfrak{A} = (0, \mathcal{A}(\rho), 0)$. Returning back to the Cartesian coordinates one obtains $\mathfrak{A} = \mathcal{A}(\rho)\big(-\sin\theta, \cos\theta, 0\big)$. The magnetic field has only the z-component which is given by

$$\mathcal{B} = \mathcal{A}' + \frac{\mathcal{A}}{\rho}, \tag{B6}$$

where prime denotes the derivative with respect to ρ. Using Eqs. (B5) and (B6), we recast the first Bogomolnyi equation (A13) in the form

$$\Phi' - \frac{\Phi}{\rho} = -\mathcal{A}\,\Phi. \tag{B7}$$

Utilizing this expression together with Eq. (B6) makes it possible to express $\mathcal{B}$ only in terms of Φ. Then, employing the second Bogomolnyi equation (A14), one obtains

$$-\Phi'' - \frac{\Phi'}{\rho} + \frac{\Phi'^2}{\Phi} - \Phi + \Phi^3 = 0. \tag{B8}$$

This equation must be solved together with the boundary conditions

$$\Phi'(0) = \mathcal{C}, \quad \Phi(\infty) = 1, \tag{B9}$$

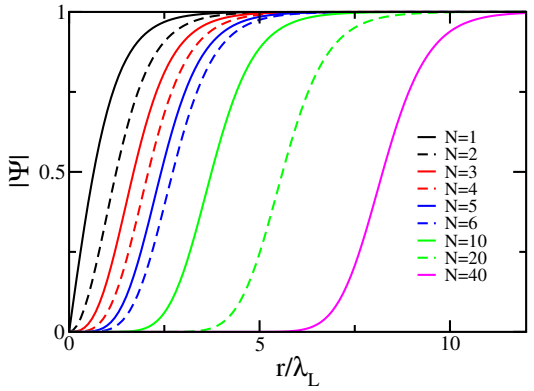

FIG. 6. (Color online) The radial part $\Phi_N(\rho)$ of the solution for an isolated multi-quantum (giant) vortex with different N.

where constant $\mathcal{C}$ should be chosen in such a way that to satisfy the second (asymptotic) condition at $\rho \to \infty$. The boundary condition for the derivative of Φ ensures that the solution has an asymptote $\Phi(\rho) \propto \rho$ in the limit $\rho \to 0$, as it should be for a single-quantum vortex.

For an isolated vortex that carries N elementary magnetic fluxes a solution is of the form

$$\Psi_N = \Phi_N(\rho)\exp(-\mathrm{i}N\theta) = (x - \mathrm{i}y)^N \frac{\Phi_N(\rho)}{\rho^N}. \tag{B10}$$

The vector potential chosen as before, to have only a single θ-component. The first Bogomolnyi equations now reads as

$$\Phi_N' - N\,\frac{\Phi_N}{\rho} = -\mathcal{A}\,\Phi_N. \tag{B11}$$

Utilizing this relation together with Eqs. (A14) and (B6), we find for Φ_N the same equation as previously for Φ. However, the boundary conditions are now different and depend on the number of flux quanta, i.e.,

$$\partial_\rho^N \Phi_N(0) = \mathcal{C}, \quad \Phi_N(\infty) = 1. \tag{B12}$$

where the first of these conditions ensures the asymptote $\Phi(\rho) \propto \rho^N$ for $\rho \to 0$. This is rather inconvenient for numerical calculations because a solution is very sensitive to $\mathcal{C}$. One can, however, rewrite this equation by introducing the new quantity

$$\phi_N = \Phi_N^{1/N}. \tag{B13}$$

Substituting it into Eq. (B8), we obtain

$$-\phi_N'' - \frac{\phi_N'}{\rho} + \frac{\phi_N'^2}{\phi_N} - \frac{\phi_N}{N} + \frac{\phi_N^{2N+1}}{N} = 0. \tag{B14}$$

Now the boundary conditions are the same as previously for Φ, i.e., $\phi_N'(0) = \mathcal{C}$ and $\phi_N(\infty) = 1$. In Fig. 6 one can see how the modulus of Ψ varies with the radial coordinate for several selected $N = 1 \ldots 40$. For the reader convenience, the data are plotted versus ρ/λ_L, where ρ is the unscaled radial coordinate here.

Appendix C: Multi-vortex configurations: long-range interaction of two vortices

Here we consider multi-vortex configurations. In particular, we rewrite the Bogomolnyi equations so that to significantly simplify analysis of a solution for an arbitrary spatial configuration of vortices (both single- and multi-quantum). To this aim we recall that the vector potential is generally given by $\mathfrak{A} = (\mathcal{A}_x, \mathcal{A}_y, 0)$ when the magnetic field has only its z-component, i.e., $\mathfrak{B} = (0, 0, \mathcal{B})$. Adopting the Coulomb gauge, $\partial_x \mathcal{A}_x + \partial_y \mathcal{A}_y = 0$, one can introduce the scalar potential φ so that

$$\mathcal{A}_x = -\partial_y \varphi, \quad \mathcal{A}_y = \partial_x \varphi. \tag{C1}$$

In this case for the magnetic field we have

$$\mathcal{B} = (\partial_x^2 + \partial_y^2)\varphi. \tag{C2}$$

Then, a solution to the first Bogomolnyi equation (A4) can be sought in the form

$$\Psi = e^{-\varphi}\, \Phi. \tag{C3}$$

Substituting this ansatz into Eq. (A4), we obtain

$$(\partial_x + \mathbb{i}\partial_y)\Phi = 0. \tag{C4}$$

This is the standard condition that Φ is an analytic function of the complex variable $Z = x + \mathbb{i}y$. The same is expressed as $\partial_{Z^*}\Phi = 0$, i.e., Φ can be an arbitrary function of Z but does not involve Z^*. The fact that Φ is an arbitrary analytic function of Z is a consequence of the infinite topological degeneracy of the Bogomolnyi point in the GL formalism at $\kappa = \kappa_0$.

Scalar potential φ obeys the equation that is obtained by inserting Eqs. (C2) and (C3) into the second Bogomolnyi equation (A14), i.e.,

$$(\partial_x^2 + \partial_y^2)\varphi = 1 - \left|\Phi\right|^2 e^{-2\varphi}. \tag{C5}$$

The boundary conditions for this equation are derived from those for the magnetic field via Eq. (C2).

Φ can easily be chosen to represent a mixed state with an arbitrary vortex spatial configuration. Indeed, the positions of vortices are defined by the zeros of Φ that fully define any analytic properties of a complex function. For example, a single vortex positioned at $\mathbf{a}$ is obviously described by $\Phi = Z - a$, where $a = a_x + \mathbb{i}a_y$. Two vortices located at $\mathbf{a}_1$ and $\mathbf{a}_2$ correspond to $\Phi = (Z - a_1)(Z - a_2)$, with $a_i = a_{i,x} + \mathbb{i}a_{i,y}$. Similarly one can construct Φ that corresponds to any spatial configuration of multiple single-quantum vortices at positions $\mathbf{a}_i$'s , i.e., $\Phi = \prod_i (Z - a_i)$, see Ref. 38. In turn, an isolated N-quantum vortex located at $\mathbf{a}$ yields $\Phi = (Z - a)^N$, etc.

A solution to Eq. (C5) can be obtained using standard numerical methods. However, one can follow a different strategy and seek a solution for a multi-vortex configuration in the form

$$\Psi = e^{-\delta\varphi} \prod_i \Psi_i, \tag{C6}$$

where Ψ_i represents the solution for an isolated N_i-quantum vortex located at $\mathbf{a}_i$. As already mentioned in the previous paragraph, Ψ_i is given by

$$\Psi_i = (Z - a_i)^{N_i} e^{-\varphi_i}, \tag{C7}$$

where φ_i satisfies

$$(\partial_x^2 + \partial_y^2)\varphi_i = 1 - |\Psi_i|^2, \tag{C8}$$

so that

$$\varphi = \delta\varphi + \sum_i \varphi_i. \tag{C9}$$

The equation for $\delta\varphi$ is obtained by substituting the ansatz of Eq. (C6) into Eq. (C5), which yields

$$(\partial_x^2 + \partial_y^2)\delta\varphi = \sum_i \left(|\Psi_i|^2 - 1\right) + 1 - \prod_i \left|\Psi_i\right|^2 e^{-2\delta\varphi}. \tag{C10}$$

Now, Eqs. (C10) and (B8) can be used to check properties of the multi-vortex configuration at long separations between vortices. From Eq. (B8) one can find that at large distances from the vortex core

$$|\Psi|^2 \approx 1 - \mathcal{D}\frac{e^{-\sqrt{2}\rho}}{\sqrt{\rho}}, \tag{C11}$$

where $\mathcal{D}$ is some constant. Substituting this into Eq. (C10) one can see that $\delta\varphi$ is exponentially small in any region sufficiently remote from the cores of vortices present in a given multi-vortex configuration (it holds for both single- and multi-quantum vortices). This makes it possible to write the ansatz given by Eq. (C6) at a point remote from any vortex core as the additive law for the magnetic field[15]

$$\mathcal{B} \approx \sum_i \mathcal{B}_i, \tag{C12}$$

where $\mathcal{B} = 1 - |\Psi|^2$ is the total magnetic field of the multi-vortex configuration and $\mathcal{B}_i = 1 - |\Psi_i|^2$ is the magnetic field created by the i-th vortex.

We further utilize the additive approximation of Eq. (C12) to investigate the long-range interaction between two vortices and calculate the corresponding integrals $\mathcal{I}$ and $\mathcal{J}$, see Eq. (25). Based on Eq. (C12), the integrand of $\mathcal{I}$ in Eq. (25) writes as

$$|\Psi|^2\big(1 - |\Psi|^2\big) \approx |\Psi_1|^2\big(1 - |\Psi_1|^2\big) + |\Psi_2|^2\big(1 - |\Psi_2|^2\big) - 2\mathcal{B}_1\mathcal{B}_2. \tag{C13}$$

As we are interested in the interaction between two vortices, we now select the contribution that depends on the distance between the vortices, i.e., the last term in the

right-hand-side of the above expression. So, $\mathcal{I}$ is given by

$$\mathcal{I} \approx -2\,\mathcal{P}, \quad \mathcal{P} = \int \mathcal{B}_1\mathcal{B}_2 d\mathbf{r}. \tag{C14}$$

When rearranging the integrand of $\mathcal{J}$ with Eq. (C12), one obtains

$$|\Psi|^4\big(1-|\Psi|^2\big) \approx |\Psi_1|^4\big(1-|\Psi_1|^2\big) + |\Psi_2|^4\big(1-|\Psi_2|^2\big) - 4\mathcal{B}_1\mathcal{B}_2. \tag{C15}$$

Again keeping the contribution dependent on the distance between vortices, we find

$$\mathcal{J} \approx -4\,\mathcal{P}. \tag{C16}$$

Thus, we arrive at the general result $\mathcal{J}/\mathcal{I} = 2$ for the long-range interaction of arbitrary vortices. It means that the critical GL parameter κ_{li}^* controls the onset of the long-range attractive interaction for any pair of vortices, including multi-quantum.

[1] V. Moshchalkov, M. Menghini, T. Nishio, Q. H. Chen, A. V. Silhanek, V. H. Dao, L. F. Chibotaru, N. D. Zhigadlo, J. Karpinski, Phys. Rev. Lett. **102**, 117001 (2009); J. Gutierrez, B. Raes, A. V. Silhanek, L. J. Li, N. D. Zhigadlo, J. Karpinski, J. Tempere, V. V. Moshchalkov, Phys. Rev. B **85**, 094511 (2012); P. Curran, W. M. Desoky, J. B. Laloe, and S. J. Bending, *Broken Symmetry Vortex Patterns in Disordered* MgB_2 *Thin Films*, Vth Workshop Frontiers of Superconductivity and Magnetism, Abstract book p. 16-18, Jan. 2014.

[2] L. D. Landau, *Collected Papers* (Oxford, Pergamon Press, 1965).

[3] P. G. de Gennes, *Superconductivity of Metals and Alloys* (Benjamin, New York, 1966).

[4] E. M. Lifshitz and L. P. Pitaevskii, *Statistical Physics, Part 2, Landau and Lifshitz Course of Theoretical Physics, Volume 9* (Oxford, Pergamon, 1980).

[5] E. B. Bogomolnyi and A. I. Vainstein, Sov. J. Nucl. Phys. **23**, 588 (1976).

[6] E. B. Bogomolnyi, Sov. J. Nucl. Phys. **24**, 449 (1976).

[7] R. Jackiw and E. J. Weinberg, Phys. Rev. Lett. **64**, 2234 (1990); D. Stuart, Commun. Math. Phys. **159**, 51 (1994); M. B. Hibdmarsh and T. W. B. Kibble, Rep. Prog. Phys. **58**, 477 (1995); O. K. Pashaev and Z. N. Gurkan, Theor. Math. Phys. **152**, 1017 (2007); P. Zhang and P. A. Horváthy, Phys. Rev. D **80**, 127703 (2009).

[8] C. Taubes, Commun. Math. Phys. **72**, 277 (1980); S. Gustafson, I. M. Sigal, and T. Tzaneteas, Journ. Math. Phys. **51**, 015217 (2010); L. Berlyand, O. Misiats, and V. Rybalko, Comm. Contemporary Math. **13**, 53 (2011).

[9] E. J. Weinberg, Phys. Rev. D **19**, 3008 (1979).

[10] U. Krägeloh, Phys. Lett. A **28**, 657 (1969); U. Essmann, Physica **55**, 83 (1971); D. R. Aston, R. L. W. Dubeck, and F. Rothwarf, Phys. Rev. B **3**, 2231 (1971); Kumpf, U.: Phys. Status Solidi (b) 44, 557 (1971); J. Auer and H. Ullmaier, Phys. Rev. B **7**, 136 (1973); H. W. Weber *et al.*, Physica C **161**, 272 (1989).

[11] A. E. Jacobs, Phys. Rev. Lett. **26**, 629 (1971); A. E. Jacobs, Phys. Rev. B **4**, 3016, (1971); A. E. Jacobs, Phys. Rev. B **4**, 3022 (1971); A. E. Jacobs, Phys. Rev. B **4**, 3029 (1971).

[12] A. Hubert, Phys. Status Solidi (b) **53**, 147 (1972).

[13] U. Klein, Journ. Low Temp. Phys. **69**, 1 (1987).

[14] P. Miranović and K. Machida, Phys. Rev. B **67**, 092506 (2003).

[15] I. Luk'yanchuk, Phys. Rev. B **63**, 174504 (2001).

[16] L. Neumann and L. Tewordt, Z. Phys. **189**, 55 (1966); L. Neumann and L. Tewordt, Z. Phys. **191**, 73 (1966).

[17] E. H. Brandt and M. P. Das, J. Supercond. Nov. Magn. **24**, 57 (2011).

[18] E. Babaev and M. Speight, Phys. Rev. B **72**, 180502(R) (2005); E. Babaev, J. Carlström and M. Speight, Phys. Rev. Lett. **105**, 067003 (2010); J. Carlström, E. Babaev, and M. Speight, Phys. Rev. B **83**, 174509 (2011).

[19] V. G. Kogan and J. Schmalian, Phys. Rev. B **83**, 054515 (2011), see also the comment in E. Babaev and M. Silaev, ibid. 86, 016501 (2012) and the reply V. G. Kogan and J. Schmalian, ibid. 86, 016502 (2012).

[20] A. A. Shanenko, M. V. Milošević, F. M. Peeters, and A. V. Vagov, Phys. Rev. Lett. **106**, 047005 (2011); A. Vagov, A. A. Shanenko, M. V. Milošević, V. M. Axt, F. M. Peeters, Phys. Rev. B **86**, 144514 (2012).

[21] V. H. Dao, L. F. Chibotaru, T. Nishio, and V. V. Moshchalkov, Phys. Rev. B **83**, 020503 (2011); A. Chaves, L. Komendova, M. V. Milosevic, J. S. Andrade, G. A. Farias, and F. M. Peeters, Phys. Rev. B **83**, 214523 (2011); S.-Z. Lin and X. Hu, Phys. Rev. B **84**, 214505 (2011).

[22] G. E. Volovik and L. P. Gor'kov, Sov. Phys.-JETP 61, 843 (1985) [Zh. Eksp. Teor. Fiz. 88, 1412 (1985)].

[23] M. Sigrist and K. Ueda, Rev. Mod. Phys. **63**, 239 (1991).

[24] A. V. Vagov, A. A. Shanenko, M. V. Milošević, V. M. Axt, F. M. Peeters, Phys. Rev. B **85**, 014502 (2012).

[25] The special case of symmetric bands requires a separate consideration. Its results will be published elswhere.

[26] A. Hubert, Phys. Lett. A 36, 359 (1971).

[27] U. Krey, Phys Lett. A **37**, 421 (1971).

[28] A. E. Jacobs, Phys. Lett. A **38**, 153 (1972).

[29] L. Kramer, Z. Physik **258**, 367 (1973); M. C. Leung and A. E. Jacobs, J. Low Temp. Phys. **11**, 395 (1973); M. C. Leung, J. Low Temp. Phys. **12**, 215 (1973).

[30] N. V. Orlova, A. A. Shanenko, M. V. Milošević, F. M. Peeters, A. V. Vagov, and V. M. Axt, Phys. Rev. B **87**, 134510 (2013).

[31] B. T. Geilikman, R. O. Zaitsev and V. Z. Kresin, Solid State Phys. **9**, 642 (1967) [in Russian, Fizika Tverdogo

Tela **9**, 821 (1967)]; V. Z. Kresin, Journal of Low Temp. Phys. **11**, 519 (1973).

[32] A. A. Golubov, J. Kortus, O. V. Dolgov, O. Jepsen, Y. Kong, O. K. Andersen, B. J. Gibson, K. Ahn, and R. K. Kremer, J. Phys.: Condens. Matter **14**, 1353 (2002).

[33] Y. Singh, C. Martin, S. L. Bud'ko, A. Ellern, R. Prozorov, and D. C. Johnston, Phys. Rev. B **82**, 144532 (2010).

[34] R. Khasanov, M. Bendele, A. Amato, K. Conder, H. Keller, H.-H. Klauss, H. Luetkens, and E. Pomjakushina, Phys. Rev. Lett. **104**, 087004 (2010).

[35] H. Kim, M. A. Tanatar, Y. J. Song, Y. S. Kwon, and R. Prozorov, Phys. Rev. B **83**, 100502(R) (2011).

[36] A. Brinkman, A. A. Golubov, H. Rogalla, O. V. Dolgov, J. Kortus, Y. Kong, O. Jepsen, and O. K. Andersen, Phys. Rev. B **65**, 180517(R)(2002).

[37] S. Borisenko, Nature Mater. **12**, 600 (2013).

[38] B. A. Dubrovin and S. P. Novikov, Sov. Phys. JETP **52**, 511 (1980) [in Russian, Zh. Eksper. Teor. Fiz. **79**, 1006 (1980)].